JOURNAL OF SPACECRAFT AND ROCKETS
Vol. 41, No. 4, July–August 2004

Optimal Low-Thrust Trajectories Combined with an Aeroassist Maneuver

Aaron J. Trask*
Naval Research Laboratory, Washington, D.C. 20375
and
Victoria L. Coverstone†
University of Illinois at Urbana–Champaign, Urbana, Illinois 61801

Various optimal powered aeroassisted orbit transfers using solar electric propulsion are presented. These trajectories use a combination of solar electric propulsion and controlled atmospheric perturbations. Single revolution coplanar and plane change trajectories are considered. The objective of the coplanar trajectory is to circularize the orbit, and the objective of the plane change trajectory is to maximize the reduction in orbital inclination. Optimal trajectories are presented for both cases to show the benefits of combining atmospheric perturbations and solar electric propulsion.

Nomenclature

$a, e, i, \Omega, \omega, \upsilon$	=	classical orbital elements: semimajor axis a, km; eccentricity e, inclination i, deg; longitude of the ascending node Ω,°; argument of periapse ω, deg; and the true anomaly υ, deg
C_D	=	drag coefficient
C_{D0}	=	minimum drag coefficient
C_L	=	lift coefficient
c	=	exhaust velocity, m/s
D	=	drag force, N
h_{atmos}	=	altitude of negligible atmosphere, m
$h_{\min}$	=	minimum altitude, m
h_r	=	reference altitude, m
h_s	=	spacecraft altitude, m
K	=	induced drag coefficient
L	=	lift force, N
m	=	mass of the spacecraft, kg
p, f, g, h, k, L	=	modified equinoctial orbital elements
$\dot{Q}$	=	heating rate, W/cm^2
$\dot{Q}_{\max}$	=	maximum heating rate, W/cm^2
r	=	radius magnitude, m
r_p	=	periapsis, m
$\boldsymbol{r}, \boldsymbol{v}$	=	radius and velocity vector, m and m/s
S	=	reference area, m^2
T	=	thrust magnitude, N
u_r, u_θ, u_h	=	radial; tangential, and normal thrust direction cosines
V	=	velocity magnitude, m/s
v_c	=	circular orbit velocity at sea level, m/s
α	=	angle of attack, deg
β	=	inverse of the scale height, m^{-1}
γ	=	flight path angle, deg
$\boldsymbol{\Delta}$	=	perturbing acceleration vector, m/s^2
$\boldsymbol{\Delta}_A$	=	atmospheric perturbing acceleration vector, m/s^2
$\boldsymbol{\Delta}_T$	=	thrust acceleration vector, m/s^2
$\Delta_r, \Delta_\theta, \Delta_h$	=	perturbing accelerations in the radial, tangential, and normal directions, m/s^2
ζ	=	out-of-plane thrust angle, deg
η	=	in-plane thrust angle, deg
μ	=	gravitational constant, m^3/s^2
ρ	=	atmospheric density, kg/m^3
ρ_r	=	reference density, kg/m^3
ρ_0	=	density at sea level, kg/m^3
σ	=	bank angle, deg

Received 23 May 2003; revision received 9 July 2003; accepted for publication 24 July 2003.

*Aerospace Engineer, Code 8103, 4555 Overlook Avenue S.W. Member AIAA.

†Associate Professor, 306 Talbot Laboratory, MC-236, 104 S. Wright Street. Associate Fellow AIAA.

Introduction

SOLAR electric propulsion (SEP) and aeroassist technologies are enabling technologies of future space exploration missions. Recently, the Deep Space 1 (DS1) spacecraft successfully demonstrated the use of SEP for interplanetary missions. Aeroassist technologies were used for the Magellan spacecraft about Venus and recently for the Mars Global Surveyor spacecraft. Many future missions may use both of these technologies to save propellant mass and reduce transfer times.

Aeroassisted orbit transfers to reduce fuel consumption were pioneered by London[1] in 1962. Since that time, many papers have been published on the subject. Munk and Powell[2] explained some of the aeroassist technologies and their usefulness in future missions. Aerobraking uses atmospheric drag to change the spacecraft's orbit. This procedure was implemented on the Mars Global Surveyor over a period of nine months in order to lower the apoapse from an altitude of 56,000 km to 400 km, saving approximately 1200 m/s of velocity change in fuel. Aerocapture uses a single atmospheric pass to change the orbit from a hyperbolic arrival trajectory to an elliptic capture trajectory. Powell[3] and Striepe et al.[4] discuss the use of aerocapture and precision landing in the future Mars Surveyor Program. Precision landing is guided aeroentry, which the Space Shuttle routinely performs. Lohar et al.[5] presented results of an aerogravity assist around the planet Venus with heating rate considerations. Aerogravity assist uses the atmosphere and the planets' gravity to perform a larger bend angle, allowing smaller planets to be as effective as larger planets in providing velocity change.

Vinh and Hanson[6] presented results on optimal aeroassisted orbit transfers from high Earth orbit. In 1981, an extensive work by Vinh[7] presented various optimal atmospheric trajectories. Recently, Rao et al.[8] presented optimal aeroassisted orbit transfers from low Earth orbit to geostationary orbit with a large plane change. A work by Naidu[9] presented the formulation and results of aeroentry, aeroassisted, and guidance problems as well as aerocruise. Aerocruise uses thrust to cancel the drag term, leaving the lift vector to achieve plane changes without loss of orbital energy or altitude changes.

Lohar et al.[10] also presented the aerocruise problem for a coplanar minimum fuel case without a heating rate constraint and Lee and Hull[11] presented this for an optimal plane change with a heating rate constraint.

The heating constraint is an important consideration in planning future missions. The accelerations produced by the atmosphere around a planet also increase the spacecraft temperatures, which can cause damage to onboard systems. Seywald[12] applies Pontryagin's minimum principle to an aeroassisted minimum energy loss trajectory with a heating rate constraint, and Horie and Conway[13] present the results of optimal aeroassisted orbital interceptions with a heating rate constraint. Wetzel and Moerder[14] show optimal aerocapture trajectories at Mars with a convective heating constraint.

The objective of this paper is to combine the technologies of SEP with aerobraking to achieve optimal orbit transfers about the planet Mars. Owing to the recent increase in interest and the multiple planned missions, Mars was chosen as the focus of this work. This combination will be useful in evaluating these technologies and planning future missions to Mars and can be extended to other planets.

Problem Formulation

Equinoctial orbital elements are a set of nonsingular orbital elements that overcome the difficulties associated with the singularities that occur with classical orbital elements.[15] One set of these that are valid for all types of orbits are the modified equinoctial orbital elements. The modified equinoctial orbital elements in terms of the classical elements are defined by the following[15]:

$$p = a(1 - e^2) \tag{1}$$

$$f = e\cos(\omega + \Omega) \tag{2}$$

$$g = e\sin(\omega + \Omega) \tag{3}$$

$$h = \tan(i/2)\cos\Omega \tag{4}$$

$$k = \tan(i/2)\sin\Omega \tag{5}$$

$$L = \Omega + \omega + v \tag{6}$$

The differential equations for the modified equinoctial orbital elements are[16]

$$\dot{p} = (2p/w)\sqrt{p/\mu}\Delta_\theta \tag{7}$$

$$\dot{f} = \sqrt{p/\mu}\{\Delta_r \sin L + [(w+1)\cos L + f](\Delta_\theta/w) - (h\sin L - k\cos L)(g\Delta_h/w)\} \tag{8}$$

$$\dot{g} = \sqrt{p/\mu}\{-\Delta_r \cos L + [(w+1)\sin L + g](\Delta_\theta/w) + (h\sin L - k\cos L)(f\Delta_h/w)\} \tag{9}$$

$$\dot{h} = \sqrt{p/\mu}\left(s^2\Delta_h/2w\right)\cos L \tag{10}$$

$$\dot{k} = \sqrt{p/\mu}\left(s^2\Delta_h/2w\right)\sin L \tag{11}$$

$$\dot{L} = \sqrt{\mu p}(w/p)^2 + (1/w)\sqrt{p/\mu}(h\sin L - k\cos L)\Delta_h \tag{12}$$

where

$$w = 1 + f\cos L + g\sin L \tag{13}$$

$$s^2 = 1 + h^2 + k^2 \tag{14}$$

The perturbing acceleration due to the atmosphere of Mars and the thrusting of the spacecraft for this problem is

$$\boldsymbol{\Delta} = \boldsymbol{\Delta}_A + \boldsymbol{\Delta}_T \tag{15}$$

The assumption of a spherical nonrotating atmosphere for Mars is made in this paper. This gives a simple exponential equation for the density of the Martian atmosphere[17]:

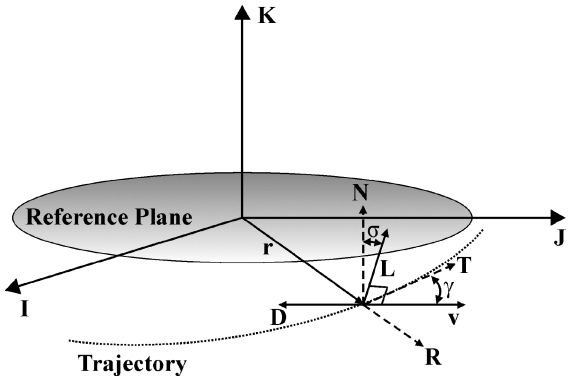

Fig. 1 Atmospheric forces on the spacecraft.

$$\rho = \rho_r \exp[-\beta(h_s - h_r)] \tag{16}$$

The forces on the spacecraft introduced by the atmosphere are the drag force opposite to the velocity vector and the lift force perpendicular to the velocity vector and rotated about the velocity vector by the bank angle as depicted in Fig. 1[18]:

$$D = \tfrac{1}{2}\rho S C_D(\alpha)V^2 \tag{17}$$

$$L = \tfrac{1}{2}\rho S C_L(\alpha)V^2 \tag{18}$$

The drag coefficient is modeled with a parabolic drag polar[18]:

$$C_D = C_{D0} + K C_L(\alpha)^2 \tag{19}$$

In the radial-tangential-normal coordinates, the atmospheric perturbing accelerations become

$$\boldsymbol{\Delta}_A = \frac{L}{m}\begin{bmatrix}\sin\sigma\cos\gamma\\ \sin\sigma\sin\gamma\\ \cos\sigma\end{bmatrix} + \frac{D}{m}\begin{bmatrix}-\sin\gamma\\ -\cos\gamma\\ 0\end{bmatrix} \tag{20}$$

$$\sin\gamma = \frac{\boldsymbol{r}^T\boldsymbol{v}}{rV} \tag{21}$$

Flight through the Martian atmosphere introduces a heating rate $\dot{Q}$, which is defined as follows[12,19]:

$$\dot{Q} = 19,987.49\sqrt{\rho/\rho_0}(v/v_c)^{3.15}\ \text{W/cm}^2 \tag{22}$$

This heating rate is important to maintain at a level appropriate for the thermal control system of the spacecraft to dissipate. If this does not occur the spacecraft will suffer damage and possible loss of operability.

The perturbing acceleration for a thrusting spacecraft and the additional differential equation for the change in mass are

$$\boldsymbol{\Delta}_T = \frac{T}{m}\begin{bmatrix}u_r\\ u_\theta\\ u_h\end{bmatrix} \tag{23}$$

$$\dot{m} = -\frac{T}{c} \tag{24}$$

A nonlinear programming (NLP) algorithm, FMINCON from MATLAB, is used to determine optimal control parameter values for the given problem subject to the constraints. FMINCON finds the minimum of a scalar function subject to linear and nonlinear constraints. It uses a sequential quadratic programming (SQP) method that closely mimics Newton's method for unconstrained optimization.[20]

The atmospheric trajectories have one linear and two nonlinear constraints. The linear constraint consists of bounds on the control

Table 1 Physical properties

Property	Value
h_{atmos}	150 km
$h_{\min}$	50 km
A	11.69 m^2
C_{D0}	0.032
K	1.4
m	4837.9 kg
ρ_r	7.8×10^{-4} kg/m^3
h_r	31.800×10^3 m
β	10^{-4} m^{-1}
ρ_0	0.020 kg/m^3
v_c	3.5528 km/s

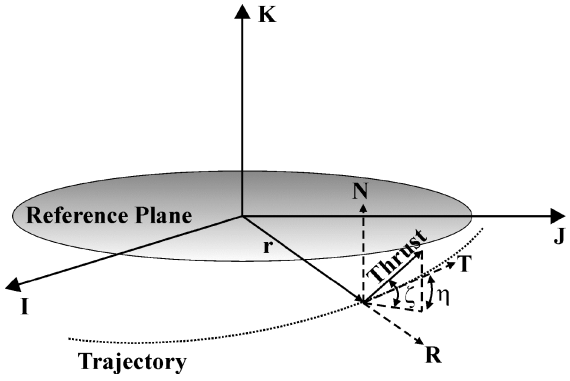

Fig. 2 Thrust direction parameters.

parameter C_L. The upper and lower bounds are given by the geometry of the vehicle. For this paper, they were selected as shown in Eq. (25):

$$0 \le C_L \le 1 \tag{25}$$

The constraints for the minimum altitude and maximum heating rate are nonlinear in terms of the modified equinoctial elements:

$$h_s \ge h_{\min} \tag{26}$$

$$\dot{Q} \le \dot{Q}_{\max} \tag{27}$$

The properties of a typical atmospheric transfer orbit vehicle (ATOV) are shown in Table 1 along with minimum altitude and the altitude at which the atmosphere is assumed negligible at Mars.[12]

The NSTAR (NASA Solar Electric Propulsion Technology Application Readiness Program) ion thruster used on DS1 was chosen for the simulations. This gives an approximate mass flow rate $\dot{m} = 1.2272$ mg/s and thrust $T = 35.084$ mN, using a power of 1.0308 kW and the equations in Refs. 21 and 22.

The thrust direction was determined by the choice of an in-plane angle referenced to the local horizontal and an out-of-plane angle (Fig. 2). A set of equal-time-spaced thrust directions was determined, and a spline was used in the same fashion as the atmospheric controls segment. This was done in order to interpolate the thrust direction during numerical integration. The thrust acceleration is described in the following form:

$$\boldsymbol{\Delta}_T = \frac{T}{m} \begin{bmatrix} \cos\zeta \sin\eta \\ \cos\zeta \cos\eta \\ \sin\zeta \end{bmatrix} \tag{28}$$

and the constraints on the new control parameters are

$$-180 \text{ deg} \le \eta \le 180 \text{ deg} \tag{29}$$

$$-180 \text{ deg} \le \zeta \le 180 \text{ deg} \tag{30}$$

For each case the full set of modified equinoctial orbital element differential equations is used. The thrust is on only during those portions of the trajectory outside of the atmosphere in order to alleviate the physical coupling of the atmospheric controls and the thrust pointing controls. The coefficient of lift and bank angle are chosen for the atmospheric portion of the trajectory, and the thrust angle parameter values are chosen for the remainder of the trajectory. The chosen values are then interpolated between to provide a continuous input to the full modified equinoctial element differential equations, which are then integrated using a fourth-order Runge–Kutta integrator. The Hermite cubic spline was chosen for its ability to interpolate plateaus in the data as well as reducing undulation in the interpolation. The Hermite cubic spline uses calculated slopes at each data point to aid in reducing undulation when compared with a cubic spline. The slope values were determined from each point's forward neighbor and setting the slope to zero at the maximum and minimum allowed values. If undulation in the interpolant is not reduced, the optimizer would select control parameters such that significant overshoot would occur above the constrained maximum value, thereby producing the undesirable effect of violating the constraint for periods of time.

Coplanar Circularization Results

Single-revolution coplanar optimal low-thrust aeroassisted trajectories about the planet Mars are considered. The goal of the optimal trajectory is to circularize the orbit while maintaining the periapse at the same altitude. This is achieved by minimizing the final value of the eccentricity subject to the periapse at the initial time equal to the periapse at the final time.

For the coplanar cases, the bank angle is set to -90 deg and the out-of-plane thrust angle is set to 0 deg to maintain a coplanar trajectory, whereas the coefficient of lift and the in-plane thrust angle are allowed to vary. The NLP FMINCON chooses optimal values of the parameters C_L and η at 15 equally spaced time nodes. The parameter C_L is chosen for the atmospheric portion of the trajectory. Owing to a lack of a priori knowledge of this time period, an estimate is used. This estimate starts with the atmospheric entry time and ends with the projected atmospheric exit time of an unperturbed trajectory. Additional minutes are included in the estimate to allow for a possible longer atmospheric phase due to perturbations in the trajectory. The parameter η is chosen for a time period of the atmospheric entry time to one period of the initial orbit. During altitudes within the atmosphere, the thrust is turned off. The time is referenced to the periapse passage of the initial unperturbed orbit. Atmospheric control parameters are chosen only for one atmospheric pass, and so for large times where the spacecraft may enter the atmosphere again, accelerations due only to the propulsion system and not to atmospheric acceleration terms are modeled.

Two sets of initial orbital elements shown in Table 2 are used. The trajectory is started at atmospheric entry and ends after one period based on the initial elements from Table 2. The first set with the maximum heating rate of 556.5 W/cm^2 has an optimal solution as shown in Figs. 3 and 4. The vertical lines in the plots represent the atmosphere entry and exit points, and time is referenced to periapse passage of the initial unperturbed orbit. For the atmospheric portion of the trajectory, C_L starts at low values in order not to violate the heating rate constraint. After the maximum heating rate occurs around the initial periapse, C_L rises to a constant value of 1.0 in order to lower the apoapse. The segment of the spline for C_L that dips below zero due to undulation is negligible. For the thrusting portion of the trajectory, the in-plane thrust angle starts at -180 deg in order to lower the apoapse and then raises the periapse to the

Table 2 Initial orbit properties

Property	First set	Second set
a	5209.5 km	3831.3 km
e	1/3	1/11
r_p	3473 km	3483 km
Period	190 min	120 min

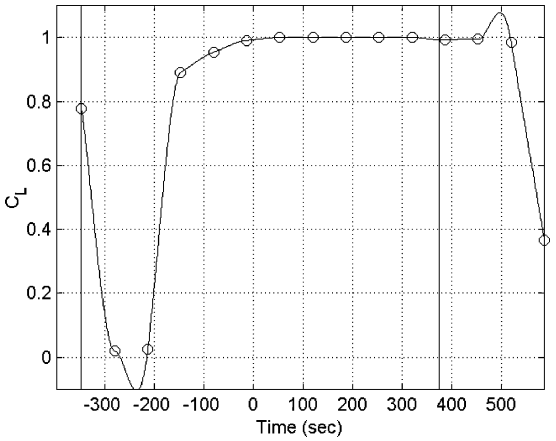

Fig. 3 Time history of the coefficient of lift: $\dot{Q}_{\max} = 556.5$.

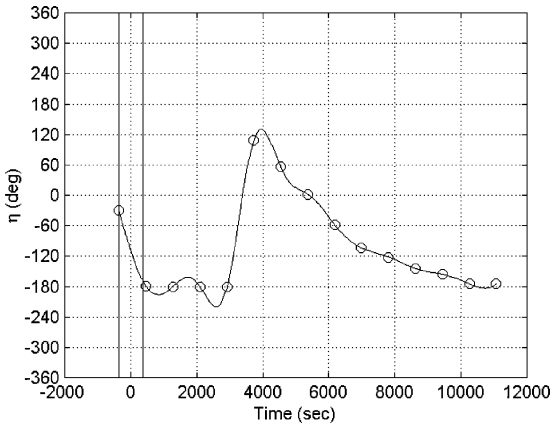

Fig. 4 Time history of the in-plane thrust angle: $\dot{Q}_{\max} = 556.5$.

initial periapse in the second half of the trajectory. This uses 0.0131 kg of propellant mass, which saves propellant mass over thrusting for the entire trajectory without atmospheric perturbations for the same initial orbital elements. This savings comes at no cost and actually produces 135% greater change in eccentricity, which produces a less elliptic orbit.

For the same initial elements but with no maximum heating rate constraint, the optimal solution is the parameter C_L chosen at 1.0 for the entire atmospheric portion of the trajectory. A similar time history of the in-plane thrust angle occurs as in the preceding constrained case. This gives a $\Delta e = -0.0539$, which is an improvement over the constrained case with no additional mass expended and a maximum heating rate of 565 W/cm^2. Table 3 compares these results with those of the thrust-only case.

The second set of initial orbital elements shown in Table 2 has an optimal solution, with a maximum heating rate of 238.5 W/cm^2, as shown in Figs. 5 and 6. The control parameters have a time history similar to that in the preceding case. This gives a $\Delta e = -0.0202$, which reduces the eccentricity more than the thrust-only case, as seen in Table 4. This occurs with no added cost and saves 0.0016 kg of propellant mass.

For the same initial elements but with no maximum heating rate constraint, the NLP selects the parameter C_L optimally at 1.0 and the in-plane thrust angle has a similar time history. This gives a $\Delta e = -0.0285$, which is an improvement over the constrained case with no additional mass expended and a maximum heating rate of 256.4 W/cm^2. Table 4 compares these results with those of the thrust-only case.

Plane Change Results

Single-revolution optimal low-thrust aeroassisted trajectories with a plane change about the planet Mars are also considered. The

Table 3 Result comparison: $\dot{Q}_{\max} = 565$

Case	Δe	$\Delta\varepsilon$, km^2/s^2	Δm, kg
Unconstrained	−0.0539	−0.3322	−0.0131
Constrained	−0.0510	−0.3142	−0.0131
Thrust only	−0.0217	−0.1338	−0.0140

Table 4 Result comparison: $\dot{Q}_{\max} = 256.4$

Case	Δe	$\Delta\varepsilon$, km^2/s^2	Δm, kg
Unconstrained	−0.0285	−0.1751	−0.0072
Constrained	−0.0202	−0.1244	−0.0072
Thrust only	−0.0149	−0.0919	−0.0088

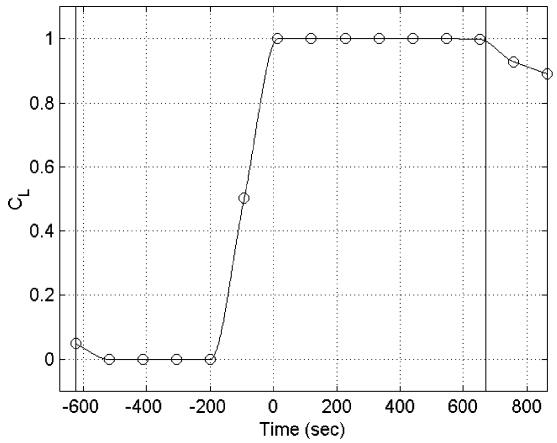

Fig. 5 Time history of the coefficient of lift: $\dot{Q}_{\max} = 238.5$.

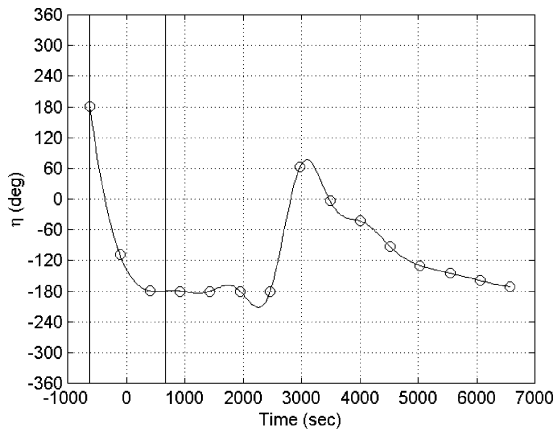

Fig. 6 Time history of the in-plane thrust angle: $\dot{Q}_{\max} = 238.5$.

goal of the optimal trajectory is to perform a plane change toward an equatorial Martian orbit while maintaining the periapse at the same altitude. This is achieved by minimizing the change in inclination subject to the equality constraint of the initial periapse equal to the final periapse.

The bank angle and out-of-plane thrust angle are allowed to vary in order to achieve a plane change. The NLP chooses optimal values of the control parameters at 15 nodes as in the preceding section. The same spline methods are used as before to interpolate the control parameters.

The two sets of initial orbital elements outlined in Table 2 are used with an added initial inclination of 30 deg. The trajectory is started at the atmospheric entry time and ends after one period corresponding to the initial orbital elements. The first set, with a maximum heating rate of 511 W/cm^2, has an optimal solution as shown in Figs. 7–10. The atmospheric controls vary as in the plane change trajectories shown previously. However, the thrust angles do not vary as before.

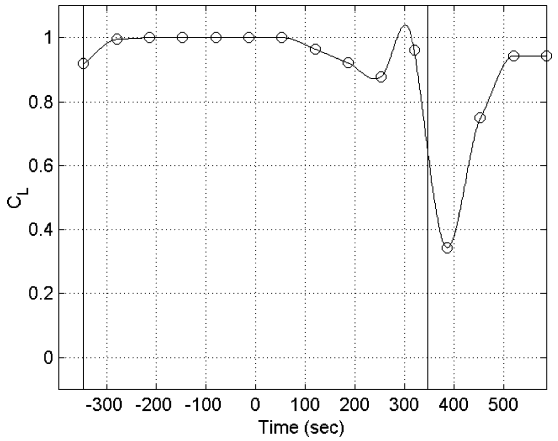

Fig. 7 Time history of the coefficient of lift: $\dot{Q}_{\max} = 511$.

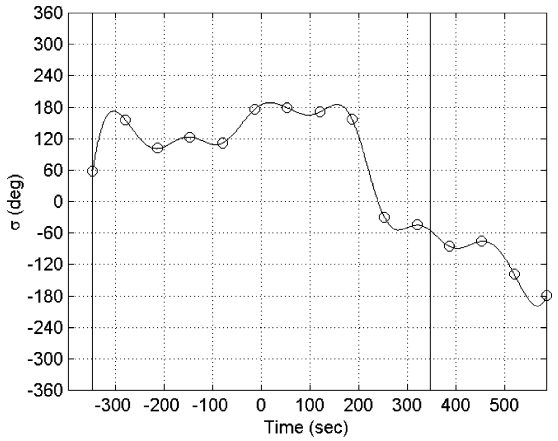

Fig. 8 Time history of the bank angle: $\dot{Q}_{\max} = 511$.

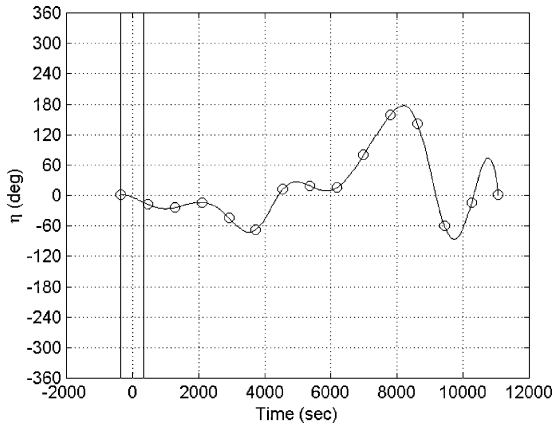

Fig. 9 Time history of the in-plane thrust angle: $\dot{Q}_{\max} = 511$.

This is due to the drag term during the atmosphere pass creating an eccentricity change and lowering the periapse. The thrust must correct the periapse change outside of the atmosphere as well as add an additional change in the inclination. The aeroassisted solution gives a $\Delta i = -0.8763$ deg, which is 32.2% less inclination change than in the thrust-only case. This is due to the thrust required to correct the periapse after the atmosphere pass because the thrust is off during the atmosphere pass and cannot cancel the drag term.

For the same initial elements but with no maximum heating rate constraint, the optimal solution is similar to the planar case. The parameter C_L is chosen to be 1.0 for the atmospheric portion of the trajectory, and the bank angle and thrust angles have time histories similar to those of the constrained case, yielding a $\Delta i = -0.9880$ deg and a maximum heating rate of 533 W/cm^2. This is an improvement over the constrained case, as shown in Table 5.

Table 5 Result comparison: $\dot{Q}_{\max} = 533$

Case	Δe	Δi, deg	$\Delta\varepsilon$, km^2/s^2	Δm, kg
Unconstrained	−0.0326	−0.9880	−0.2012	−0.0132
Constrained	−0.0313	−0.8768	−0.1929	−0.0132
Thrust only	0.0019	−1.2925	0.0118	−0.0140

Table 6 Result comparison: $\dot{Q}_{\max} = 238.6$

Case	Δe	Δi, deg	$\Delta\varepsilon$, km^2/s^2	Δm, kg
Unconstrained	−0.0153	−0.4220	−0.0940	−0.0072
Constrained	−0.0147	−0.4062	−0.0901	−0.0072
Thrust only	0.0007	−0.4860	0.0046	−0.0088

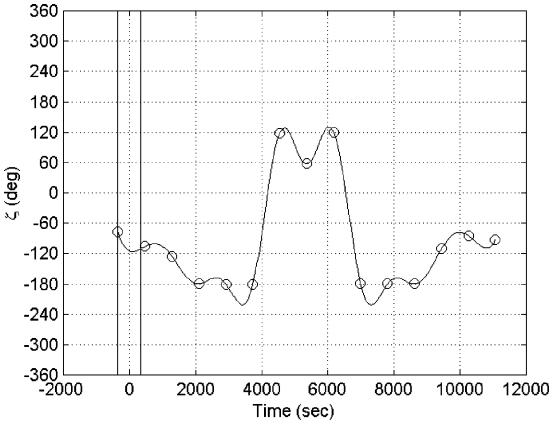

Fig. 10 Time history of the out-of-plane thrust angle: $\dot{Q}_{\max} = 511$.

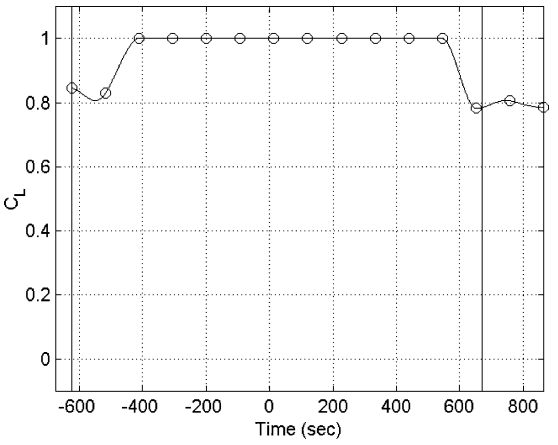

Fig. 11 Time history of the coefficient of lift: $\dot{Q}_{\max} = 232.8$.

The second set of initial orbital elements has an optimal solution, with a maximum heating rate of 232.8 W/cm^2, as shown in Figs. 11–14. A similar control history occurs as before, yielding a $\Delta i = -0.4062$ deg. The reduction in inclination change is due to the same reasons as mentioned previously but is much closer to the thrust-only case solution due to the size of the initial orbit and the shortened period.

Again, for the same initial elements but with no maximum heating rate constraint, the optimal solution is similar to that of the preceding unconstrained case. This gives a $\Delta i = -0.4220$ deg, which is a slight improvement over the constrained case but is still less than the thrust-only case while achieving a maximum heating rate of 238.6 W/cm^2. Table 6 compares these results with those of the thrust-only case.

The formulation of the problem was sensitive to the initial guess of the control parameters given to the NLP. Using results obtained

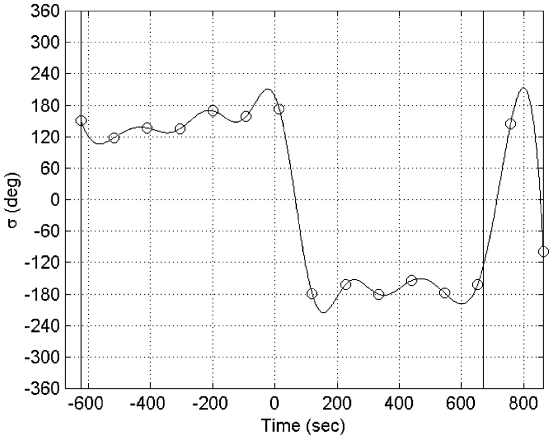

Fig. 12 Time history of the bank angle: $\dot{Q}_{\max} = 232.8$.

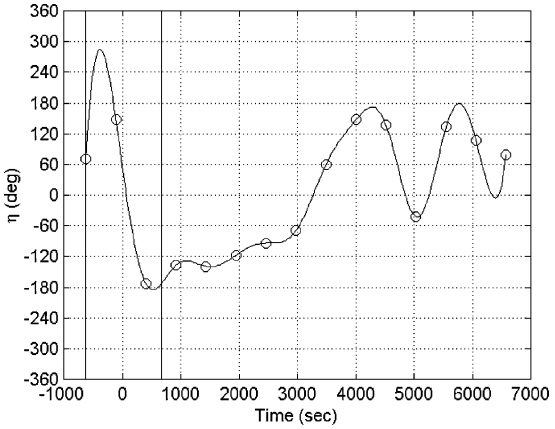

Fig. 13 Time history of the in-plane thrust angle: $\dot{Q}_{\max} = 232.8$.

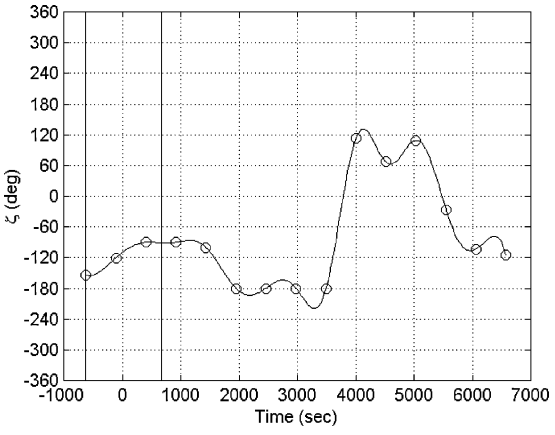

Fig. 14 Time history of the out-of-plane thrust angle: $\dot{Q}_{\max} = 232.8$.

from preceding runs as a starting point decreased the computational time required to find the optimal solution. The software could be modified to allow a greater variety of orbit transfers and cost functions. The difficulty lies in predicting when the atmosphere control parameters are needed and when the thrust control parameters are needed. Multiple atmospheric passes as well as initial orbital elements outside of the atmosphere are possible, but a priori knowledge of the number of atmospheric passes required to complete the mission objectives is needed.

Conclusions

The results of optimal low-thrust aeroassisted spacecraft trajectories around the planet Mars were presented. First, optimal trajectories were determined to lower the eccentricity of the initial elliptical orbit. As expected, these trajectories achieved a smaller final eccentricity than when only thrusters were used, showing the advantages in performing aeroassist maneuvers in combination with SEP. Second, optimal trajectories were determined for a plane change. Using atmospheric perturbations for purely a plane change resulted in lower performance than thrusting alone. This was due to the reduction of eccentricity that occurred during the atmospheric portion of the trajectory and the constraints imposed on the final periapse remaining unchanged from its initial value. Outside of the atmosphere the thrust vector raised the final periapse to the initial periapse but in doing so reduced its effectiveness for inclination change.

References

[1]London, H. S., "Change of Satellite Orbit Plane by Aerodynamic Maneuvering," *Journal of the Aerospace Sciences*, Vol. 29, No. 3, 1962, pp. 323–332.

[2]Munk, M. M., and Powell, R. W., "Aeroassist Technology Planning for Exploration," American Astronautical Society, AAS Paper 2000-169, Jan. 2000.

[3]Powell, R. W., "Numerical Roll Reversal Predictor–Corrector Aerocapture and Precision Landing Guidance Algorithms for the Mars Surveyor Program 2001 Missions," AIAA Paper 98-4574, Aug. 1998.

[4]Striepe, S. A., Queen, E. M., Powell, R. W., Braun, R. D., Cheatwood, F. M., Aguirre, J. T., Sachi, L. A., and Lyons, D. T., "An Atmospheric Guidance Algorithm Testbed for the Mars Surveyor Program 2001 Orbiter and Lander," AIAA Paper 98-4569, Aug. 1998.

[5]Lohar, F. A., Mateescu, D., and Misra, A. K., "Optimal Atmospheric Trajectory for Aero-Gravity Assist," *Acta Astronautica*, Vol. 32, No. 2, 1994, pp. 89–96.

[6]Vinh, N. X., and Hanson, J. M., "Optimal Aeroassisted Return from High Earth Orbit with Plane Change," *Acta Astronautica*, Vol. 12, No. 1, 1985, pp. 11–25.

[7]Vinh, N. X., *Optimal Trajectories in Atmospheric Flight*, Elsevier Scientific, New York, 1981.

[8]Rao, A. V., Tang, S., and Hallman, W. P., "Numerical Optimization of Multiple-Pass Aeroassisted Orbital Transfer," *Optimal Control Applications and Methods*, Vol. 23, No. 4, 2002, pp. 215–238.

[9]Naidu, D. S., "Aeroassisted Orbital Transfer: Guidance and Control Strategies," *Lecture Notes in Control and Information Sciences*, Vol. 188, Springer-Verlag, London, 1994.

[10]Lohar, F. A., Sherwani, A. K., and Misra, A. K., "Transfer Between Coplanar Elliptical Orbits Using Aerocruise," *Journal of Guidance, Control, and Dynamics*, Vol. 21, No. 6, 1998, pp. 971–974.

[11]Lee, J. Y., and Hull, D. G., "Maximum Orbit Plane Change with Heat-Transfer-Rate Considerations," *Journal of Guidance, Control, and Dynamics*, Vol. 13, No. 3, 1990, pp. 492–497.

[12]Seywald, H., "Variational Solutions for the Heat-Rate-Limited Aeroassisted Orbital Transfer Problem." *Journal of Guidance, Control, and Dynamics*, Vol. 19, No. 3, 1996, pp. 686–692.

[13]Horie, K., and Conway, B. A., "Optimal Aeroassisted Orbital Interception," *Journal of Guidance, Control, and Dynamics*, Vol. 22, No. 5, 1999, pp. 625–631.

[14]Wetzel, T. A., and Moerder, D. D., "Vehicle/Trajectory Optimization for Aerocapture at Mars," *Journal of Astronautical Sciences*, Vol. 42, No. 1, 1994, pp. 71–89.

[15]Battin, R. H., *An Introduction to the Mathematics and Methods of Astrodynamics*, AIAA, New York, 1987, pp. 490–494.

[16]Betts, J. T., "Optimal Interplanetary Orbit Transfers by Direct Transcription," *Journal of the Astronautical Sciences*, Vol. 42, No. 3, 1994, pp. 247–268.

[17]Smith, R. S., Mease, K. D., Bayard, D. S., and Farless, D. L., "Aeromaneuvering in the Martian Atmosphere: Simulation-Based Analyses," *Journal of Spacecraft and Rockets*, Vol. 37, No. 1, 2000, pp. 139–142.

[18]Hull, D. G., Giltner, J. M., Speyer, J. L., and Mapar, J., "Minimum Energy-Loss Guidance for Aeroassisted Orbital Plane Change," *Journal of Guidance, Control, and Dynamics*, Vol. 8, No. 4, 1985, pp. 487–493.

[19]Chapman, D. R., "An Approximate Analytical Method for Studying Entry into Planetary Atmospheres," NACA TN-4276, May 1958.

[20]Coleman, T., Branch, M. A., and Grace, A., *Optimization Toolbox User's Guide*, Ver. 2, The MathWorks, Inc., Natick, MA, 1999.

[21]Williams, S. N., and Coverstone-Carroll, V. L., "Mars Missions Using Solar Electric Propulsion," *Journal of Spacecraft and Rockets*, Vol. 37, No. 1, 2000, pp. 71–77.

[22]Williams, S. N., and Coverstone-Carroll, V. L., "Benefits of Solar Electric Propulsion for the Next Generation of Planetary Exploration Missions," *Journal of the Astronautical Sciences*, Vol. 45, No. 2, 1997, pp. 143–159.

D. Spencer
Associate Editor